Electrochemical studies of tri-manganese substituted Keggin-ions.

Authors: Jochen Friedl [a,b], Rami Al-Oweini [c], Max Herpich [a,b], Ulrich Kortz [c],

Ulrich Stimming [a,b,d,1*]

Affiliations:

[a] TUM CREATE Centre for Electromobility, 1 CREATE Way, CREATE Tower, Singapore 138602, Singapore

[b] Department of Physics E19, Technische Universität München, James-Franck Str. 1, 85748 Garching, Germany

[c] Jacobs University

[d] Institute for Advanced Study (IAS) of the Technische Universität München, Lichtenbergstr. 2a, 85748 Garching, Germany

* Corresponding author. Tel.: +65 65923013 / Fax: + 65 68969950. E-mail address: ulrich.stimming@tum-create.edu.sg (U. Stimming)

[1] ISE Member

Abstract

1. Introduction

Polyoxometalates (POMs) are discrete metal-oxo anions of early transition-metals in high oxidation states representing a unique class of inorganic cage complexes [1]. They show an enormous range of different shapes, sizes and compositions and are relevant to a multiplicity of research areas such as catalysis, biology, medicine and materials science [2].

Of special versatility are Keggin- and Wells-Dawson-type polyanions as they can release one or more WO_6 units and thereby form lacunary derivatives. Transition metals can be coordinated by terminal and basic oxygens of these lacunaries which introduces electrophilic centers into the molecules [3–5]. Lacunary precursors can therefore be regarded as inorganic ligands with vacant sites and attaching transition metals to these can introduce additional functionality into the POM.

This added functionality can be harnessed for electrochemical applications. Recently, Pratt et al. employed the tri-vanadium substituted Keggin-type redox-couple $(SiV^{V}_{3}W^{VI}_{9}O_{40})^{7-}$ /$(SiV^{IV}_{3}W^{VI}_{9}O_{40})^{10-}$ in the positive half-cell of a redox flow battery. Redox characteristics of the three inserted V^{V}-ions are added to those of the nine W^{VI} - ions [6]. For application in electrochemical supercapacitors it was reported that the addition of $PMo^{VI}_{10}V^{V}_{2}O_{40}$ to a conductive polymer led to an increased pseudocapacitance [7].

In this article we report the electrochemistry of the tri-Mn substituted Keggin-ions $K_7[Mn^{II}_3(OH)_3SiW_9O_{34}(H_2O)_3]$ $(Mn^{II}_3SiW_9)$[2] and $K_4[Mn^{III}_3(OH)_3SiW_9O_{34}(H_2O)_3]$ $(Mn^{III}_3SiW_9)$ in aqueous solution. We will also briefly discuss cyclic voltammograms (CVs) of the parent heteropolyacid $H_4[SiW_{12}O_{40}]$ (SiW_{12}) and its lacunary derivatives $K_8[SiW_{11}O_{39}]^{8-}$ (SiW_{11}), $K_{10}[SiW_9O_{34}]$ (SiW_9) and the mono-Mn substituted Keggin-ion $K_6[Mn^{II}SiW_{11}O_{39}(H_2O)]$ $(Mn^{II}_1SiW_{11})$ to showcase the changes with proceeding WO_6 loss and Mn insertion.
The electron transfer reactions were investigated in different electrolytes as it was reported that $Mn^{II}_1SiW_{11}$ can undergo ligand exchange [8]. Furthermore, the pH value was varied to investigate whether the POMs undergo proton or cation coupled heterogeneous electron transfer

[2] For clarity cations, oxygen atoms and water or hydroxyl groups will be omitted in the short notation.

[9]. To obtain insights into the kinetics of the electron transfer we investigated the oxidation of Mn^{III} to Mn^{IV} in $Mn^{III}{}_3SiW_9$ with a potentiostatic single pulse (PSP) method at different temperatures. As a study using an electrochemical quartz crystal microbalance (EQCM) showed that Mn-containing POMs adsorb at carbon electrodes we scanned a Highly Ordered Pyrolithic Carbon (HOPG) with an Atomic Force Microscope (AFM) after immersing it into $Mn^{II}{}_3SiW_9$ containing solution at varied potentials to visualize the electrode surface [10]. In a symmetric electrolysis cell we oxidized the $Mn^{III}{}_3SiW_9$ in one half-cell while simultaneously reducing $Mn^{III}{}_3SiW_9$ in the other half-cell. With ultraviolet-visible spectroscopy (UV-VIS) the reduced and oxidized electrolytes were investigated and compared to the spectra of synthesized $SiW_9Mn^{II}{}_3$. The stability of the electrolytes was monitored after 24 hours.

2. Experimental

2.1 POM synthesis and characterization

Need assistance from Rami. Possibly only point to paper.

2.2 Electrochemical characterization

2.3

Ultra-pure type I water was obtained from an ELGA Option-Q water purification system and used to prepare the supporting electrolyte containing additionally 0.5 M Li_2SO_4 (Sigma Aldrich, ≥ 99.99 %) and 20 mM buffer solution. Buffer was either sodium acetate buffer, prepared from CH_3COOH (Sigma Aldrich, glacial, ≥ 99.99 %) and $NaCH_3COO$ (Sigma Aldrich, ≥ 99 %), or sodium citrate buffer, prepared from $C_6H_8O_7$ (Sigma Aldrich, ≥ 99.5 %) and tri-sodium citrate (Ajax Finechem, ≥ 99.0 %). To adjust the pH diluted H_2SO_4 (Sigma Aldrich, ≥ 99.99 %) was titrated into the solution. For the Mercury/Mercourus Sulfate reference electrode in sat. K_2SO_4 (MSE, 0.640 V vs. Normal Hydrogen Electrode (NHE)) the electrolyte was prepared from K_2SO_4 (Sigma Aldrich, ≥ 99 %).

CVs and PSPs were conducted in a custom-built three electrode glass cell in which a gold – wire was used as counter electrode and a MSE served as reference electrode. All potentials are given recalculated to NHE. Working electrode (WE) was a commercial glassy carbon (GC) electrode with a diameter of 1.6 mm. The electrode was polished with alumina slurry (50 nm particles) followed by silica slurry (7 nm particles) on polishing cloth. In between steps the electrode was rinsed with ultra-pure water. The glass cell was double-jacketed and temperature controlled water was pumped around the main chamber while the reference electrode was kept at ambient temperature. The water temperature was controlled and pumped with a Julabo F26-ED refrigerated-heating circulator. If the temperature is not explicitly given it was kept at 298 K.

For controlled potential electrolysis a custom-built h-type cell was used. It employed one WE in each half-cell and a MSE was inserted into one of the two compartments. The potential was measured in between the MSE and the WE in the same compartment while the current was measured in between the two WEs. Graphite paper (X2 Labwares, carbon content >99.9%) with

a geometrical surface area of 2.0 cm^2 or GFA felt from SGL carbon served as anode and cathode. To separate the two half-cells but allow for ionic conductivity a 5 % agar (Sigma Aldrich, for microbiology) which was gelled in 3.5 M KCl (Sigma-Aldrich, ≥ 99.0 %) was inserted.
For AFM measurements the working electrode was ZYH quality HOPG from VEECO which was cleaned with adhesive tape prior to usage.
Prior to each measurement the electrolyte was purged for 20 minutes with argon to remove dissolved oxygen from the solution and blanketed with argon during the course of the experiment.
A Bio-Logic SP-300 potentiostat was used for potential control and data acquisition. AFM micrographs were taken with a Bruker Multimode 8 in Scan-Assist mode. UV-VIS spectra were taken with a Cary 5000 from Agilent Technologies.

3. Results

3.1 Comparison with $Mn^{II}_1SiW_{11}$ and Reaction Mechanism

To study the reaction mechanism of $Mn^{II}_3SiW_9$ and $Mn^{III}_3SiW_9$, CVs were recorded at various scan-speeds in different electrolytes. The pH values were varied to determine whether electron transfer reactions are coupled with proton transfer [11]. As the proton concentration enters the Nernst equation as shown in Eq. (1), the equilibrium potential U_{eq} deviates from the standard potential U_0 as function of the number of transferred protons m and electrons n:

$$U_{eq} = U_0 - 0.059\ \frac{m}{n}\ pH \qquad (1)$$

U_{eq} was determined from CVs by forming the arithmetic mean of the peak potential of the oxidation U^{ox}_{peak} and reduction U^{red}_{peak}:

$$U_{eq} = \frac{U^{ox}_{peak} + U^{red}_{peak}}{2} \qquad (2)$$

Investigation of the reaction mechanism is greatly assisted by the fact that we can compare the electrochemical behavior of $Mn^{II}_3SiW_9$ and $Mn^{III}_3SiW_9$ to their parent molecule $SiW_{12}O_{40}$ (SiW_{12}) as well as to Keggin-ions containing one (SiW_{11}) or three lacunaries (SiW_9). The alpha isomer of the Keggin Tungstate SiW_{12} is one of the most studied POMs. It has a T_d symmetry and contains twelve equivalent W-ions, so-called addenda atoms, at external or peripheral positions [12].
In addition, we can resort to studies performed by Sadakane and Steckhan who elucidated the electron transfer properties of $Mn^{II}_1SiW_{11}$ [8].
CVs for all six POMs are shown in Fig. 1. The data were recorded in 20 mM sodium acetate

buffer. Scan-speed, pH and POM concentration are given in each graph.

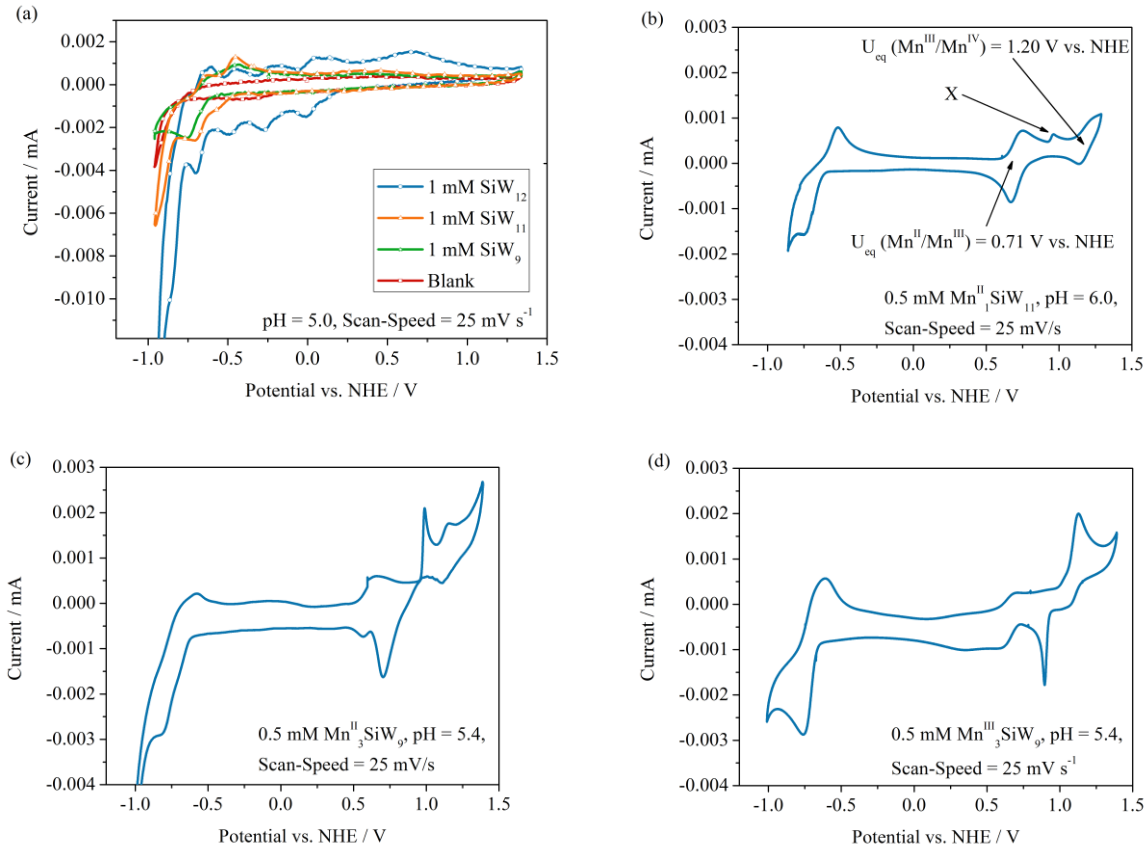

Fig. 1. (a) CVs for 1 mM of the POMs without inserted Mn ions. The parent molecule (blue curve) SiW_{12} shows considerably more redox reactions than the lacunary POMs SiW_{11} (orange curve) and SiW_9 (green curve). For comparison then plain supporting electrolyte is shown (red curve). (b) CV for 0.5 mM mono-Mn substituted Keggin ion. The peak designated with X is previously unreported in the literature. CVs for 0.5 mM (c) $Mn^{II}{}_3SiW_9$ and (d) $Mn^{III}{}_3SiW_9$. Scan-speed was 25 mV s^{-1} recorded with GC electrode with radius 0.8 mm.

Fig. 1(a) shows CVs for 1 mM of SiW_{12}, SiW_{11}, SiW_9 and a curve for the GC electrode in plain supporting electrolyte (blank). The Keggin-structure SiW_{12} was referred to as electron reservoir and it easily accepts electrons by W-ion reduction [13,14]. Added electrons are delocalized and reside equally in the twelve W-ions [15]. This manifests itself in the blue curve that shows multiple one- or two-electron redox waves that are discussed extensively in the literature [2]. Removal of one or three W-ions breaks the symmetry T_d and therefore SiW_{11} and SiW_9 show a considerably reduced redox-behavior compared to SiW_{12}. However, the three SiW_x (x = 9, 11, 12) share a common reduction wave at $U_{peak}^{red} = -0.70$ V vs. NHE and subsequent oxidation waves at $U_{peak}^{ox} = -0.62$ V vs. NHE and $U_{peak}^{ox} = -0.46$ V vs. NHE. In Fig. 1(b) a CV of $Mn^{II}{}_1SiW_{11}$ is shown. Comparison with ref. [8] and Fig. 1(a) allows to identify the two peaks

correlated to the $Mn^{II/III}$ and $Mn^{III/IV}$ redox reactions. They are marked in the graph and their U_{eq} are at 0.71 V vs. NHE and 1.20 V vs. NHE respectively. The oxidation peak marked with X has not been observed by Sadakane and Steckhan who investigated the molecule in phosphate buffer. It also has no corresponding reduction peak. The authors stated that $Mn^{II}{}_1SiW_{11}$ can undergo ligand exchange when the Mn-ion is in oxidation state Mn^{II} and that the molecule retransforms when in oxidation state Mn^{IV}. Therefore, we assign this peak to the oxidation reaction:

$$Li_3[Mn_1^{III}SiW_{11}(CH_3COOH)] \rightarrow Li_3[Mn_1^{IV}SiW_{11}(CH_3COO)] + e^- + H^+ \quad (3)$$

An Ch_3COOH-group from the buffer solution replaces the H_2O molecule in $Mn^{II}{}_1SiW_9$ prior to its oxidation to Mn^{III}, the acetate ion is again replaced by an OH^--group at Mn^{IV}.
CVs of the two tri-Mn substituted Keggin-ions are shown in Fig. 1(c) and (d). While both of them show the typical W-ion redox reactions discussed earlier, their redox-behavior at potentials higher than 0.3 V vs. NHE differs greatly from each other and from $Mn^{II}{}_1SiW_{11}$. In this potential domain only the Mn redox reactions take place and Fig. 2(a) shows these processes in greater detail.
Chemically $Mn^{II}{}_3SiW_9$ and $Mn^{III}{}_3SiW_9$ should be very similar, albeit the latter is in a higher oxidation state. In a three-electrode cell the active species is only converted within the diffusion layer close to the electrodes, the bulk is not oxidized or reduced. Therefore, all the $Mn^{II}{}_3SiW_9$ molecules can undergo ligand exchange, as the bulk is in oxidation state Mn^{II}, while for $Mn^{III}{}_3SiW_9$ only the small fraction within the diffusion layer is prone to this process when a potential corresponding to Mn^{II} is applied. In analogy to the work of Sadakane and Steckhan we propose a reaction mechansim that can explain the observed redox behavior, for which we will present thorough experimental evidence.
For the $Mn^{II/III}$ redox reaction, which is marked with II/III in Fig. 2(a), we assume the reaction to be a cation coupled electron transfer (CCET):

$$Li_7[Mn_3^{II}(OH)_3SiW_9O_{34}(L)_3] \rightleftharpoons Li_4[Mn_3^{III}(OH)_3SiW_9O_{34}(L)_3] + 3\,e^- + 3\,Li^+ \quad (4)$$

L designates the ligand and represents CH_3COOH in the case of $Mn^{II}{}_3SiW_9$ or stands for H_2O in the case of $Mn^{III}{}_3SiW_9$. As 0.5 M Li_2SO_4 was added to the supporting electrolyte we expect most of the cations to be Li^+, some K^+ might participate too. When we replaced the Li_2SO_4 in the supporting electrolyte with K_2SO_4 we observed no changes.
This CCET is very similar for the two species under investigation, L does not participate. However, the deviation is significant for the $Mn^{III/IV}$ redox reaction which is assumed to be a proton coupled electron transfer (PCET). As the protons are released or taken up by the incorporated ligand L, it influences the reaction. For $Mn^{II}{}_3SiW_9$ we get:

$$Li_4[Mn_3^{III}(OH)_3SiW_9O_{34}(CH_3COOH)_3] \rightleftharpoons Li_4[Mn_3^{IV}(OH)_3SiW_9O_{34}(CH_3COO)_3] + 3\,e^- + 3H^+ \quad (5)$$

The oxidation peak of this reaction is marked with $(III/IV)^{CH_3COOH}$ in Fig. 2(a). The cathodic current at 0.73 V vs. NHE is the corresponding reduction.
The PCET for $Mn^{III}_3SiW_9$ reads:

$$Li_4[Mn_3^{III}(OH)_3SiW_9O_{34}(H_2O)_3] \rightleftharpoons Li_4[Mn_3^{IV}(OH)_6SiW_9O_{34}] + 3\,e^- + 3H^+ \quad (6)$$

Its oxidation peak is marked with $(III/IV)^{H_2O}$ in the graph, the reduction peaks are visible at 1.09 and 0.90 V vs. NHE. Looking at Fig. 2(b), which shows a CV of $Mn^{III}_3SiW_9$ at pH 4.2 and higher scan-speed of 100 mV s^{-1} one can even distinguish three separate reduction peaks which are marked with U^1_{red}, U^2_{red} and U^3_{red}. However, the center reduction peak is not very pronounced and hard to spot in most CVs. We assume that the reducion process of equation (6) is a stepwise reduction and not a three-electron redox process.
Fig. 2(c) shows a qualitative analyzis of the oxidation peak of same redox reaction. The experimental data (orange scatter) is compared to simulated curves. Simulation parameters electrode-area, concentration of active species, scan-speed and temperature match the experimental details. For the electron transfer constant k_0 we assumed a fairly high value of k_0 = 0.01 cm s^{-1} and the diffusion constant D we estimated at D = 2.56 10^{-6} cm s^{-2}, as reported for the Keggin-ion [16]. The red curve, which is the simulated value for a concerted three-electron oxidation differs greatly from the experimental data. The peak-current is higher and the general shape does not match as the onset for the experimental curve is at lower potentials. Three thin, blue lines designate one-electron oxidation currents which differ only in a 10 mV offset in their U_{eq}. The superimposition of those three lines, the thick blue line, leads to a curve that matches the experimental data very well. Therefore, we assume that the oxidaiton reaction of equation (6) proceeds via three separate one-electron transfers, too.
Both POMs show smaller redox-waves at potentials at which the other molecule undergoes its characteristic reactions. For example $Mn^{III}_3SiW_9$ exhibits a small oxidation current at the potential of the $(III/IV)^{CH_3COOH}$ peak, before its main oxidation wave takes place. Similarily $Mn^{II}_3SiW_9$ shows a cathodic current at U = 1.11 V vs. NHE close to the first reduction peak U^1_{red}. This supports the hypothesis that the difference between the two CVs is caused by ligand-exchange. Some of the $Mn^{II}_3SiW_9$ molecules retain their H_2O-group and therefore show redox reactions characteristic of $Mn^{III}_3SiW_9$ and vice versa.

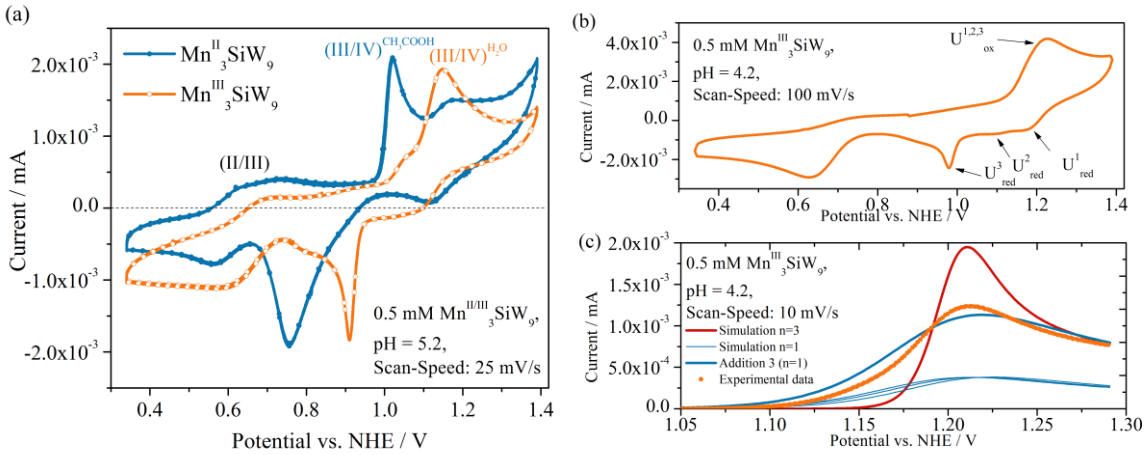

Fig. 2. (a) CVs for 0.5 mM of $Mn^{II}{}_3SiW_9$ and $Mn^{III}{}_3SiW_9$ focusing on the Mn redox reaction for direct comparison. The Mn oxidation peaks $(III/IV)^{CH_3COOH}$ and $(III/IV)^{H_2O}$ are named according to their participating ligand group (eq. (5) and eq. (6)).

3.2 Dependence on pH and supporting electrolyte

The Pourbaix diagram in Fig. 3 gives U_{eq} over pH value for the reactions described in (4), (5) and (6) and for the corresponding $Mn^{II}{}_1SiW_{11}$ reactions. For $Mn^{II}{}_1SiW_{11}$ an additional data-point was taken at pH 1.8 that matches the dashed linear fit and is omitted for clarity. In our experiments we saw that $Mn^{II}{}_3SiW_9$ and $Mn^{III}{}_3SiW_9$ decompose at pH < 3.5. The empty symbols give U_{eq} for the Mn^{II}/Mn^{III} redox reactions. $Mn^{II}SiW_{11}$ exhibits this redox reaction at a potential which is roughly 50 mV higher than the $Mn^{II/III}$ reaction of the tri-substituted Keggin-ions. None of the molecules shows a dependence on the pH value. This is either consistent with a pure electron transfer or a CCET mechanism. As CCETs were reported for multiple mono-substituted Keggin-ions, including $Mn^{II}{}_1SiW_{11}$, we assume that the $Mn^{II}/^{III}$ redox reaction is coupled to cation transfer. This mechanism can be explained by ion-pairing of the highly-charged POM and cations of the supporting electrolyte [8,17,18].

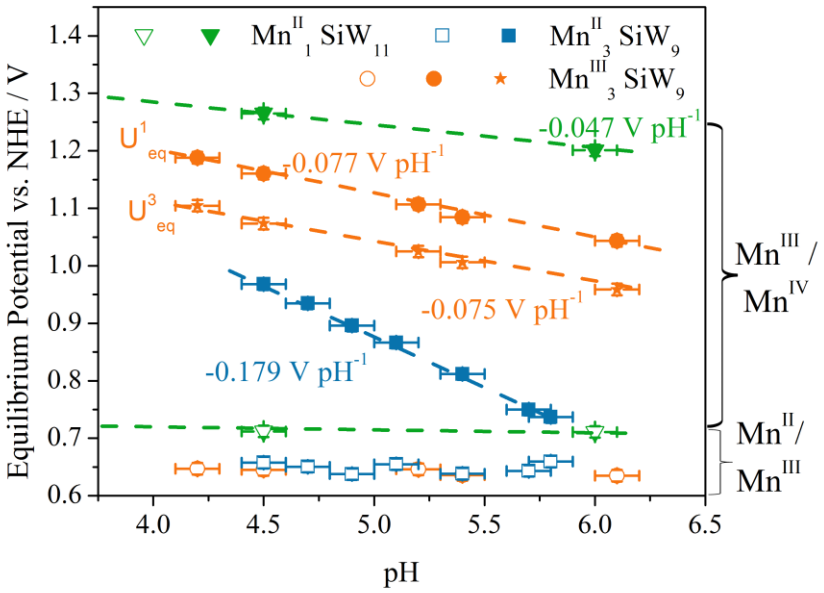

Fig. 3. Pourbaix diagram which gives the equilibrium potential over pH value for redox reactions of $Mn^{II}_1SiW_{11}$, $Mn^{II}_3SiW_9$ and $Mn^{III}_3SiW_9$. Empty symbols designate the $Mn^{II/III}$ reactions while full symbols represent the $Mn^{III/IV}$ reactions. For $Mn^{III}_3SiW_9$ two equilibrium potentials are given (U^1_{eq} and U^3_{eq}). They are calculated with the reduction potential U^1_{red} and U^3_{red} from Fig. 2(c).

The $Mn^{III/IV}$ redox reactions exhibit a dependence on the pH value. For $Mn^{II}SiW_{11}$ U_{eq} changes by -0.047 V pH^{-1} which is lower than the theoretical value of -0.059 V pH^{-1} for a one electron-one proton redox reaction. It is also lower than the value of -0.057 V pH^{-1} found by Sadakane and Steckhan [8].
For $Mn^{III}_3SiW_9$ we calculated two equilibrium potentials using equation (2). While the position of the oxidation peak is the same we used the first reduction peak U^1_{red} (1.09 V vs. NHE in Fig. 2(a)) for U^1_{eq} marked with full circles in Fig. 2(b). The data marked with full stars U^3_{eq} is the arithmetic mean of the oxidation peak and the pronounced reduction peak U^3_{red} at 0.90 V vs. NHE. For both U_{eq} the dependence on the proton concentration is quite similar, they shift with 0.077 V pH^{-1} and 0.075 V pH^{-1} respectively.
The strongest influence of the pH was found for the $Mn^{III/IV}$ redox reaction of $Mn^{II}_3SiW_9$. When protons are released (taken up) from the CH_3COOH-groups (acetate ions) U_{eq} changes with -0.179 V pH^{-1}. This implies that three protons are involved per electron in the PCET, as the theoretical slope for that kind of mechanism is -0.177 V pH^{-1}.

To further investigate the ligand exchange we replaced the acetic acid buffer in the supporting electrolyte with phosphoric acid buffer or citric acid buffer. CVs of $Mn^{II}_3SiW_9$ in the three different supporting electrolytes are shown in Fig. 4(a). The potential range was chosen to be one that only shows the $Mn^{II/III}$ and $Mn^{III/IV}$ reactions. While the green line, which was recorded in

H_3PO_4, shows some faradaic reactions it certainly does not show the peaks we assigned to equation (5), which involves CH_3COOH-group. For the orange line, which was recorded in citric acid buffer, hardly any reduction reaction was observed at a scan-speed of 25 mV s^{-1}. In Fig. 4(b) CVs at higher scan-rates in the citric acid buffer are shown. For ease of comparison the current was normalized by division with the square-root of scan-speed. The oxidation peak is shifted to higher potentials for increased scan-speeds as expected due to kinetic and ohmic effects. A reduction peak is only visible at scan-speeds 500 mV s^{-1} and 1000 mV s^{-1}. This indicates that the species formed by oxidation is unstable and decays on the time-scale of some milliseconds. Both results, the absence of peaks assigned to CH_3COOH/CH_3COO^- in phosphate buffer and the unstable species in citric acid buffer, indicate that the anion of the supporting electrolyte is incorporated into the POMs at oxidation state Mn^{II}. As $C_6H_8O_7$ is a bulkier than $C_2H_4O_2$ it is well conceivable that incorporation of the former influences the POM framework more than the latter.

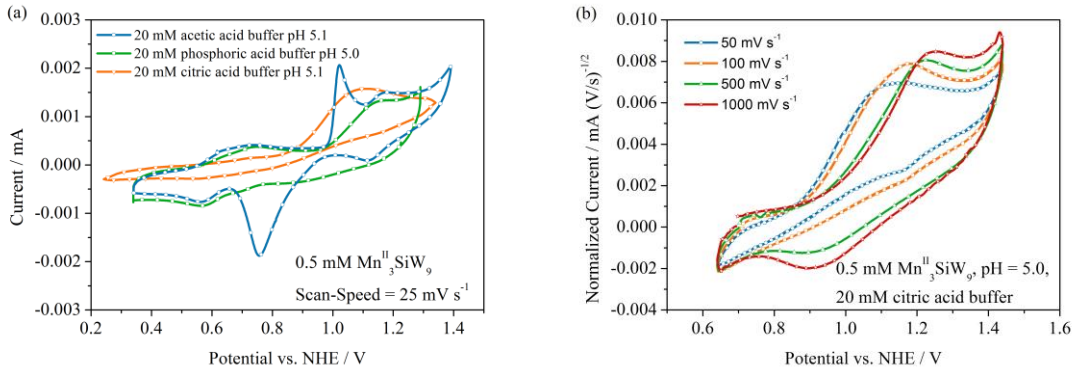

Fig. 4. (a) CVs for 0.5 mM of $Mn^{II}_3SiW_9$ in three different buffer solutions. As oxidation state Mn^{II} is prone to ligand exchange the supporting electrolyte has an influence on the curves. (b) CVs for 0.5 mM of $Mn^{II}_3SiW_9$ in citric acid buffer at different scan-speeds with normalized current. A reduction peak is only visible for 500 mV s^{-1} and 1000 mV s^{-1}.

3.3 Number of transferred electrons

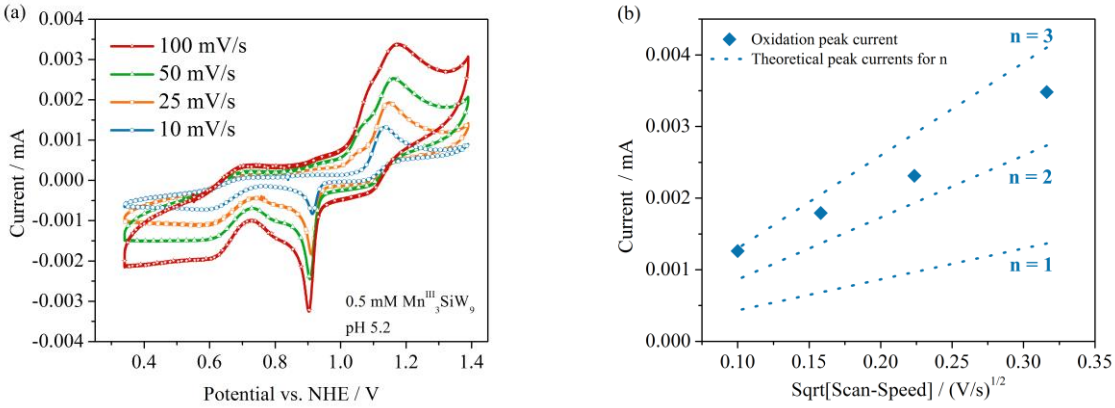

Fig. 5. (a) CVs for 0.5 mM of $Mn^{III}_3SiW_9$ in acetic acid buffer solutions at different scan-speeds. (b) Comparison of experimentally determined peak currents for the oxidation of $Mn^{III}_3SiW_9$ with curves calculated from eq. (7). Ordinate is the square-root of scan-speed.

In Fig. 2(c) we showed how CV-simulation can be used to get a qualitative idea about the number of transferred electron n during the oxidation reaction of eq. (6). In addition, the Randles-Sevcik equation can be employed to get a numeric value for n:

$$I_{peak} = 2.69\ 10^5\ n^{3/2} A\ c\ (D\ \nu)^{1/2} \qquad (7)$$

It predicts a linear dependence of the peak current I_{peak} on the square-root of scan-speed ν [19]. In addition the electrode surface area A, the concentration of active species c and the already introduced D enter the equation. There are certain caveats which need to be observed when using this equation. First, the equation only holds for infinitely fast redox-kinetics, for more sluggish electron transfer reactions it is an approximation. Second, while the geometric electrode area is known, the true surface area A is not. By thorough electrode polishing we tried to diminish that source of error as much as possible. Fig. 5(a) shows CVs of $Mn^{III}_3SiW_9$ at different scan-rates. The reaction we are investigating is the oxidation of Mn^{III} to Mn^{IV} which is coupled to proton release from a water group. Its peak potential is located at 1.13 V vs. NHE for 10 mV s^{-1}. A plot of the determined I_{peak} over the square-root of scan-speed is shown in Fig. 5(b). To simplify the evaluation we also plotted eq. (7) for n = 1, 2, 3. The experimental data lies in between the lines for n = 2 and n = 3. For 10 mV s^{-1} the data point matches the theoretical curve quite well, at higher rates they deviate more. We assume that the discrepancy to n = 3 arises from the oxidation via eq. (5), the acetic acid pathway. Its oxidation wave can be clearly observed for scan-rates of 25 mV s^{-1} and faster and this parallel pathway could account for the missing current to n = 3.

3.4 Charge Transfer Kinetics

To determine the charge transfer kinetics of above reaction, the Mn^{III}_3 to Mn^{IV}_3 oxidation of $Mn^{III}_3SiW_9$, we employed PSPs. This method faces the fundamental problem that the non-faradaic charging current masks the faradaic current up to a time which is equal to $t = 5\ \tau = 5\ R_{sol}\ C_{DL}$ [20,21]. We determined the ohmic drop between reference electrode and WE to $R_{sol} = 43.6\Omega$ and the double layer capacitance to $C_{DL} = 0.654\mu F$ ($\approx 33\mu F\ cm^{-2}$) using electrochemical impedance spectroscopy. For comparison we calculated $C_{DL} = (0.542 \pm 0.054)\mu F$ ($\approx 27\mu F\ cm^{-2}$) from fast CVs in plain supporting electrolyte. These values for C_{DL} correspond well with the literature value for the specific C_{DL} of GC 24 – 36μF cm^{-2} [22]. Therefore, the time constant τ for the experimental setup is ≤ 28.5μs and all non-faradic currents have decayed after 142.6μs.

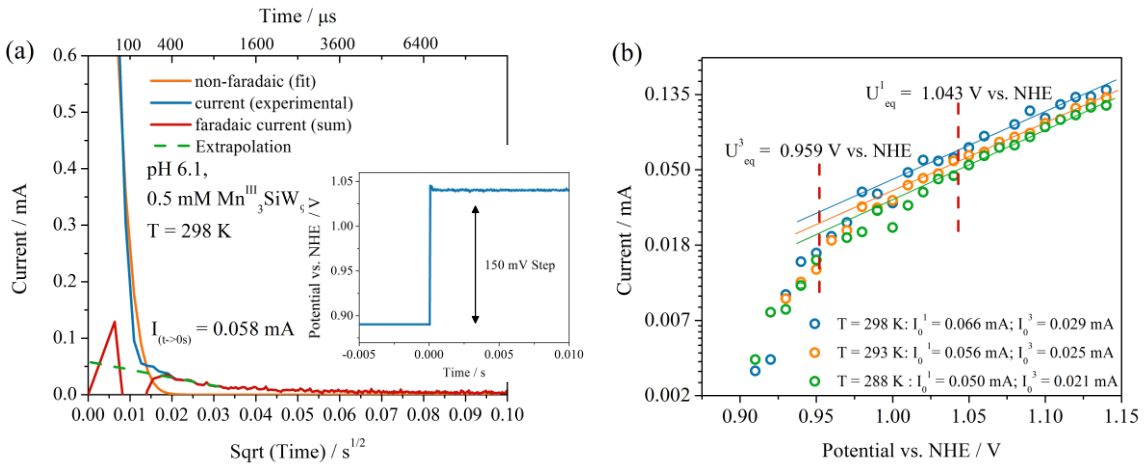

Fig. 6. (a) PSP experiment for the oxidation of $Mn^{III}_3SiW_9$, the applied potential pulse is shown in the inset. The bottom ordinate shows the square-root of time while the top ordinate shows linear time. (b) Extrapolated faradaic currents at t -> 0 s over the potential they were recorded at. Three different temperatures were investigated.

An exemplary potential program is sketched in the inset of Fig. 6(a). Until t = 0s the WE is held at a potential at which no current is measured, U = 0.89 V vs. NHE. Then the potential is stepped to a higher potential (e.g. 1.04 V vs. NHE in the example). The current response to this PSP with the square-root of time as ordinate is shown in Fig. 6(a). The blue curve shows the experimentally obtained current. For easier analysis we generated the orange curve which represents an estimation for the non-faradaic currents. It was created by fitting the first five data points to an exponential decay. The obtained $\tau = 57\mu s$ is a larger than the value we determined for the cell earlier, consequentially the orange curve decays a bit slower than the experimental current. When we subtract the non-faradaic currents from the experimental data we obtain the faradaic current which we extrapolated to t = 0s; these values were plotted over the potential at which they were obtained at for three different temperatures, which is shown in Fig. 6(b).
We found the exchange currents I^1_0 and I^3_0 by linearly extrapolating the Tafel-slopes onto their respective equilibrium potentials U^1_{eq} or U^3_{eq} as given in Fig. 3(b). These can be converted to fundamental electron transfer constants k_0 by:

$$k_0 = I_0 \, (n \, F \, A \, c)^{-1} \tag{8}$$

Assuming that three electrons are transferred we calculated $k^1_0 = 0.023$ cm s^{-1} and $k^3_0 = 0.010$ cm s^{-1} for the two equilibrium potentials. There are several sources of error, the contribution via the CH_3COOH pathway as discussed in section 3.3 and the unknown fraction of the three electrons transferred in each reaction. Thus the order of magnitude of k^1_0 and k^2_0 is more interesting than their actual values. With an order of 10^{-2} cm s^{-1} these values are comparably high which can be understood in the Marcus picture of electron transfer: As the POM-framework shields the

electrostatic interaction between polar solvent and redox-center the solvent reorganization is low which leads to facile electron transfer kinetics [23].

3.5 Adsorption on Graphite

POMs are known to interact with each other forming dimers or higher oligomers in aqueous electrolyte, despite repulsive electrostatic forces [24]. Furthermore, molecular dynamics (MD) studies predict interaction with hydrophobic materials like ionic liquids or graphite [25]. As oxidation reduces the negative charge of the Keggin-anion which in turn reduces its hydrophilic character (Born solvation model) we expect a potential dependent interaction of $Mn^{II}_3SiW_9$ and $Mn^{III}SiW_9$ with HOPG.

Aim of this study was to check for and visualize the potential dependent adsorption behavior of $Mn^{II}_3SiW_9$. For that purpose we immersed 1 cm^2 of HOPG in an electrolyte containing 50 10^{-6} M $Mn^{II}_3SiW_9$, 20 mM sodium acetate buffer at pH 5 and 0.5 M lithium sulfate. After performing electrochemical experiments the electrode was dipped in ultrapure water and investigated with an AFM.

Micrographs and one recorded CV can be seen in Fig. 7. AFM pictures were taken after immersing the HOPG at OCV (0.442 V vs. NHE) for 60s (b), after ramping the potential to 1.29 V vs. NHE (c) and after returning back to OCV (d). All three micrographs show coverage with material that is not part of HOPG and which we assign to be $Mn^{II}_3SiW_9$. While the height of the monitored particles was about 5 nm their lateral extension was always larger. Even if the lateral resolution of an AFM is limited by the width of its apex, we assume that we monitored clusters of POMs and no single molecules as reported for scanning tunneling microscope studies [26].

In Fig. 7(b) the POM was imaged in oxidation state Mn^{II}, the Keggin-anion has a formal negative charge of seven. Aggregates of molecules cover HOPG edges only; apparently the interaction of the POMs with the basal plane is too weak to resist the drag of the AFM-tip and therefore they agglomerate on the edge planes. In Fig. 7(c) the coverage is much higher than in (b); some clusters are stable on the basal plane. The inset shows a magnification of an edge plane with particles attached to it. Formal charge of the anion is negative four at this potential. The next micrograph, 7 (d) indicates that the adsorption process is potential dependent and fully reversible. When the potential is returned to U = 0.442 V vs. NHE the coverage is similar to (b) and certainly much less than in (c). Performing multiple cycles to 1.29 V vs. NHE and back to 0.442 V vs. NHE we could not detect any permanent deposition.

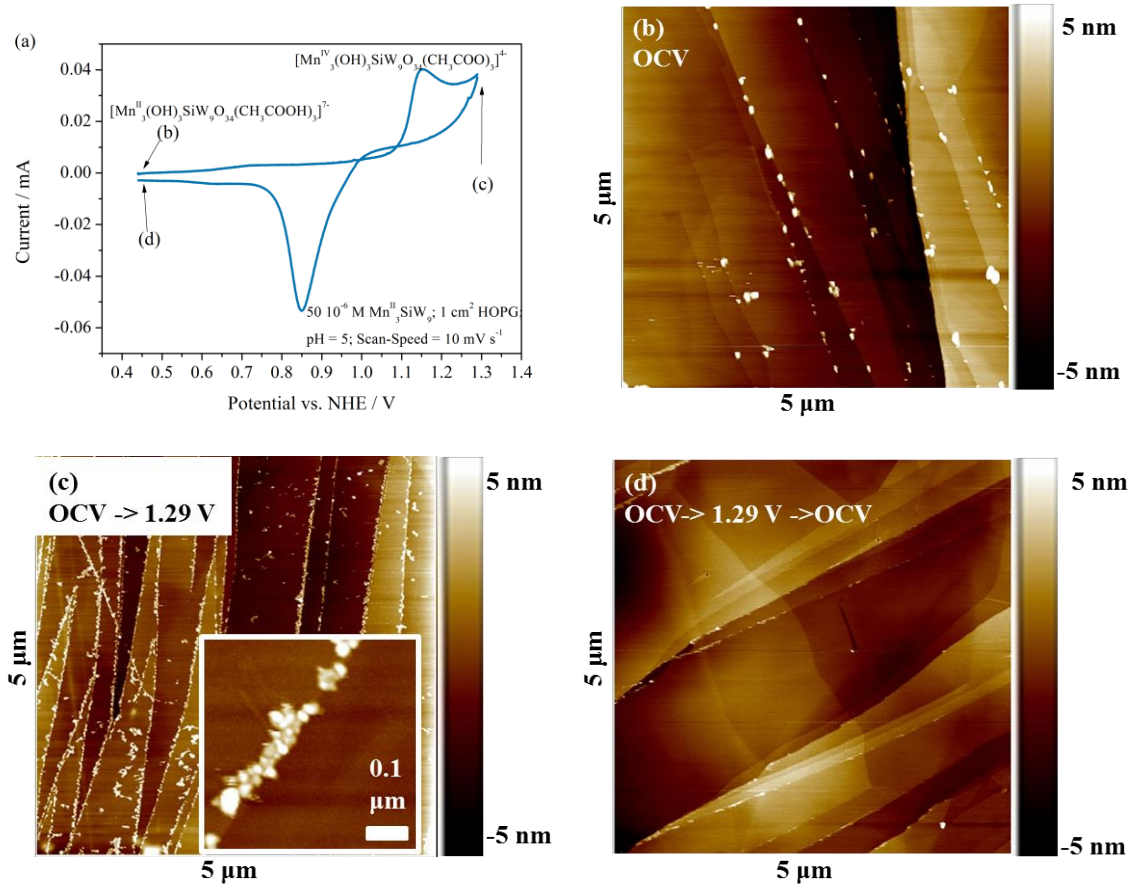

Fig. 7. (a) CV of 50 10^{-6} M $Mn^{II}_3SiW_9$ on 1 cm^2 HOPG. Oxidation states of the molecule as well as the potential positions of the AFM micrographs are given. (b) 5 µm x 5 µm micrograph recorded after immersing the HOPG at U = 0.442 V vs. NHE (OCV) for 60 s.(c) 5 µm x 5 µm micrograph recorded after performing a linear potential sweep from OCV to 1.29 V vs. NHE with 10 mV s^{-1}. The inset shows a magnification of an edge plane with attached clusters of POM.(d) 5 µm x 5 µm micrograph recorded after performing a CV from OCV to 1.29 V vs. NHE and back to OCV at 10 mV s^{-1}.

3.6 Controlled potential electrolysis

In an h-type cell we performed controlled potential electrolysis on $Mn^{III}_3SiW_9$ to investigate whether the molecule can be reduced to $Mn^{II}_3SiW_9$ and a stable Mn^{IV}_3 state can be produced simultaneously. Chronoamperometric experiments were performed using graphite paper. After the experiment we extracted the solutions from both the anode and cathode compartment and recorded their UV-VIS spectra.

The theoretical capacity of anolyte and catholyte is the product of number of transferred electrons, concentration of POMs in each solution, volume of the solution and the faraday

constant. We applied a potential of 1.29 V vs. NHE between WE and MSE and measured the current while constantly stirring the solution. The resulting current curve is displayed in Fig. 8(a). When the theoretical charge, corresponding to three electrons, was passed through the electrode we still registered a small current and kept recording. Most likely this current stems from the oxygen evolution reaction. We observed a pronounced change in color in both compartments. UV-VIS measurements are shown in Fig. 8(b). Both spectra of anolyte (solid orange curve) and catholyte (solid green curve) deviate from the solution containing $Mn^{III}{}_3SiW_9$. The orange curve, which we assign to species $Li_4[Mn^{IV}{}_3(OH)_6SiW_9O_{34}]$, shows a higher adsorption at smaller wavelengths compared to its Mn^{III} precursor, just like $Mn^{IV}{}_1SiW_{11}$ investigated by Sadakane and Steckhan [8]. When comparing the green and the red solid line, electrochemically generated $Mn^{II}{}_3SiW_9$ and synthesized $Mn^{II}{}_3SiW_9$ respectively, it is obvious that absorption profile of former is lower. This might be due to the fact that in the cathode compartment more than the theoretical charge was transferred and therefore some of the POMs in the anolyte were reduced further than to state Mn^{II}, most likely by reduction of the W-ions from W^{VI} to W^{V}. Electrolytes were stored in laboratory atmosphere and re-measured after 24 hours (dotted lines in Fig. 8(b)). The agreement with initial spectra is very high which indicates that all species are stable.

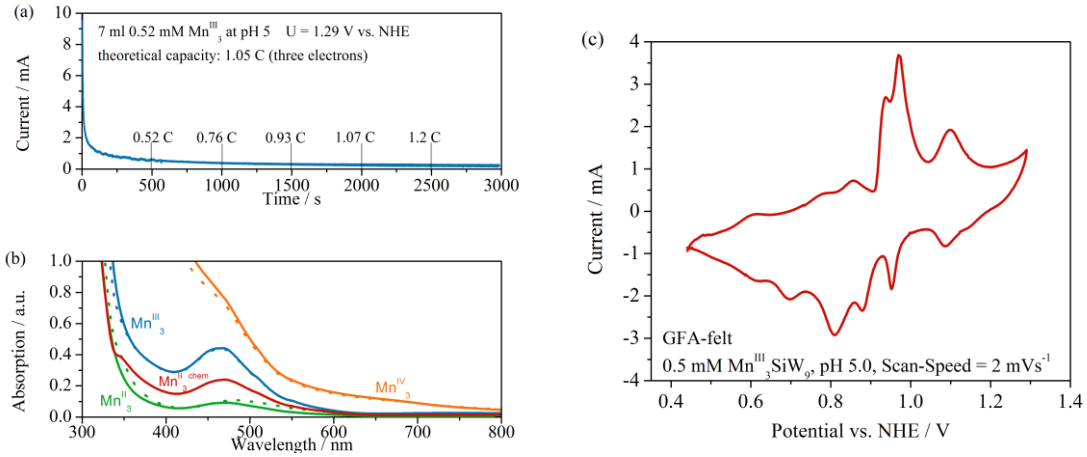

Fig. 8. (a) Current response to an applied potential of U = 1.29 V vs. NHE. (b) UV-VIS spectra of the electrochemically generated and synthesized species in oxidation states Mn^{II}, Mn^{III} and Mn^{IV}. (c) CV of $Mn^{III}{}_3SiW_9$ in the h-type cell on a high surface area, porous carbon-felt electrode.

In addition we ran a slow CV (scan-rate 2 mV s^{-1}) employing high surface area GFA-felt as working electrodes (Fig. 8(c)). Interestingly, this CV exhibits both $Mn^{II}{}_3SiW_9$- and $Mn^{III}{}_3SiW_9$-character in terms of its $Mn^{III/IV}$ redox-peaks. The peaks corresponding to eq. (5), the oxidation involving CH_3COOH/CH_3COO^-, is split into a double-peak at U = 0.935 and 0.972 V vs. NHE.

The reduction peak is a doublet with current peaks at U = 0.881 and 0.815 V vs. NHE. Also the $Mn^{II/III}$ reactions show multiple oxidation and reduction peaks. In contrast to CVs in a three-electrode setup, in this experiment the bulk is actually oxidized and reduced. Furthermore the porous geometry of the electrode impedes diffusion of species from the electrode. The CV shows both $Mn^{II}_3SiW_9$ and $Mn^{III}_3SiW_9$ features, as both species are present at the electrode.

4. Conclusions

In the present study we describe the electrochemistry of two tri-Mn substituted Keggin-ions, $Mn^{II}_3SiW_9$ and $Mn^{III}_3SiW_9$. As the molecule exhibits ligand-exchange in oxidation state Mn^{II} the anion of the supporting electrolyte is inserted into the POM which has a dramatic influence on its electrochemical behavior (e.g. Fig. 2(a)). We are not aware of an earlier publication reporting such a tremendous effect of ligand exchange. Insertion of different anions not only changes the U_{eq} of the $Mn^{III/IV}$ reaction but also renders certain oxidation states unstable.

Based on CV-studies we analyzed the redox reactions of both POMs and developed reaction equations that reflect its complex redox behavior. Fascinatingly, a CV on a high surface-area, porous graphite felt electrode shows the superposition of CVs of both $Mn^{II}_3SiW_9$ and $Mn^{III}_3SiW_9$ on polished GC electrodes (Fig. 8(c)). Analysis of the oxidation of Mn^{III} in $Mn^{III}_3SiW_9$ to Mn^{IV} indicates that all three ions are oxidized. This was qualitatively established by comparing the oxidation wave to calculated curves (Fig. 1(c)) and quantitatively by applying the Randles-Sevcik equation to calculate theoretical oxidation peak-currents (Fig. 4). Employing PSP we found that the oxidation of Mn^{III} to Mn^{IV} exhibits fast reaction kinetics with an electron transfer constant on the order of $k_0 = 10^{-2}$ cm s^{-1}.

When we imaged an HOPG surface that served as electrode we were able to confirm that the coverage of the graphite with POMs is dependent on the charge of the Keggin-anion, as predicted by MD calculations [25]. As graphite has hydrophobic properties attractive forces with anions are higher when they have a smaller formal charge. Therefore the oxidized $[Mn^{IV}_3(OH)_3SiW_9(CH_3COO)_3]^{4-}$ leads to a higher coverage of HOPG edge and basal planes than $[Mn^{II}_3(OH)_3SiW_9(CH_3COOH)_3]^{7-}$. In the monitored potential window (up to 1.29 V vs. NHE) no permanent deposition was observed and adsorption was reversible.

When performing controlled potential electrolysis at U = 1.29 V vs. NHE more than three electrons per $Mn^{III}_3SiW_9$ molecule were transferred. We think that the oxygen evolution reaction is responsible for the excess charge. This would also explain why the UV-VIS absorption spectrum of the electrochemically generated $Mn^{II}_3SiW_9$ is lower than for synthesized $Mn^{II}_3SiW_9$. The additional charge from the water oxidation led to a reduction of some W-ions from W^{VI} to W^{V}. Additionally UV-VIS measurements showed that the electrochemically generated oxidation states Mn^{II} and Mn^{IV} are stable for at least 24 hours. This might be a direct consequence of the fact that the POMs undergo CCET and PCET as those mechanism avoid high energy intermediates which enhances stability [27].

Acknowledgements

The authors would like to thank Ms. Han-Yi Chen for her help with UV-VIS measurements. This publication is made possible with the financial support from the Singapore National Research Foundation under its Campus for Research Excellence and Technological Enterprise (CREATE) program.

References

[1] U. Kortz, A. Müller, J. van Slageren, J. Schnack, N.S. Dalal, M. Dressel, Polyoxometalates: Fascinating structures, unique magnetic properties, Coord. Chem. Rev. 253 (2009) 2315–2327.

[2] M. Pope, A. Müller, Polyoxometalate chemistry: an old field with new dimensions in several disciplines, Angew. Chemie Int. Ed. …. 30 (1991) 34–48.

[3] U. Kortz, N.K. Al-Kassem, M.G. Savelieff, N.A. Al Kadi, M. Sadakane, Synthesis and Characterization of Copper- , Zinc- , Mn- , and Cobalt-Substituted Dimeric Heteropolyanions, Inorg. Chem. 40 (2001) 4742–4749.

[4] R. Al-Oweini, B.S. Bassil, T. Palden, B. Keita, Y. Lan, A.K. Powell, et al., The Mn(III)-containing tungstophosphate [MnIII3(H2O)5(A-α-PW9O34)2]9−, Polyhedron. 52 (2013) 461–466.

[5] L.C.W. Baker, J.S. Figgis, A New Fundamental Type of Inorganic Complex: Hybrid between Heteropoly and Conventional Coordination Complexes. Possibilities for Geometrical Isomerisms in 11-, 12-, 17-, and 18-Heteropoly Derivates, J. Am. Chem. Soc. 92 (1970) 3794–3797.

[6] H.D. Pratt, N.S. Hudak, X. Fang, T.M. Anderson, A polyoxometalate flow battery, J. Power Sources. 236 (2013) 259–264.

[7] A.. White, R.C.. Slade, Investigation of vapour-grown conductive polymer/heteropolyacid electrodes, Electrochim. Acta. 48 (2003) 2583–2588.

[8] M. Sadakane, E. Steckhan, Investigation of the Mn-substituted alpha-Keggin-heteropolyanion K6SiW11O39Mn(H2O) by cyclic voltammetry and its application as oxidation catalyst, J. Mol. Catal. A Chem. 114 (1996) 221–228.

[9] M. Sadakane, E. Steckhan, Electrochemical Properties of Polyoxometalates as Electrocatalysts., Chem. Rev. 98 (1998) 219–238.

[10] B. Keita, P. Mialane, F. Sécheresse, P. de Oliveira, L. Nadjo, Electrochemical generation of high-valent Mn catalysts in aqueous solutions from the sandwich-type polyoxoanion [(MnIII(H2O))3(SbW9O33)2]9−, Electrochem. Commun. 9 (2007) 164–172.

[11] D.R. Weinberg, C.J. Gagliardi, J.F. Hull, C.F. Murphy, C. a Kent, B.C. Westlake, et al., Proton-coupled electron transfer., Chem. Rev. 112 (2012) 4016–93.

[12] P. a. Aparicio, J.M. Poblet, X. López, Tungsten Redox Waves in [XMW 11 O 40] n- (X = P, Si, Al and M = W, Mo, V, Nb, Ti) Keggin Compounds - Effect of Localised/Delocalised Charges, Eur. J. Inorg. Chem. 2013 (2013) 1910–1916.

[13] G.M. Varga, B.Y.G.M.X. Arga, E. Papacoxstantinou, M.T. Pope, Heteropoly Blues . IV . Spectroscopic and Magnetic Properties of Some Reduced Polytungstates, Inorg. Chem. 9 (1970) 663.

[14] R.A. Prados, P.T. Meiklejohn, M.T. Pope, The Nature of Electron Delocalization in a Heteropoly “Blue” Anion., J. Am. Chem. Soc. 96 (1974) 1261.

[15] J.M. Maestre, X. Lopez, C. Bo, J.M. Poblet, N. Casañ-Pastor, Electronic and magnetic properties of alpha-Keggin anions: A DFT study of [XM12O40](n-), (M = W, Mo; X = Al(III), Si(IV), P(V), Fe(III), Co(II), Co(III)) and [SiM11VO40] (m- (M = Mo and W), J. Am. Chem. Soc. 123 (2001) 3749–58.

[16] M. Pope, G.M. Varga, Heteropoly blues. I. Reduction stoichiometries and reduction potentials of some 12-tungstates, Inorg. Chem. 5 (1966) 3–8.

[17] J. Toth, F. Anson, Electrochemical properties of iron (III)-substituted heteropolytungstate anions, J. Electroanal. Chem. Interfacial …. 256 (1988) 361–370.

[18] I. Weinstock, Homogeneous-phase electron-transfer reactions of polyoxometalates, Chem. Rev. 2665 (1998) 113–170.

[19] A. Bard, L. Faulkner, Electrochemical methods: Fundamentals and Applications, Second, John Wiley and Sons, New York, 2001.

[20] H. Gerischer, M. Krause, Eine Doppelimpuls-Methode zur Untersuchung sehr schneller Elektrodenreaktionen, Zeitschrift Für Phys. Chemie. 10 (1957) 264–269.

[21] T. Berzins, P. Delahay, Kinetics of fast electrode reactions, J. Am. Chem. Soc. 828 (1955) 6448–6453.

[22] R.L. McCreery, Advanced Carbon Electrode Materials for Molecular Electrochemistry, Chem. Rev. 108 (2008) 2646–2687.

[23] D. V Matyushov, Solvent reorganization energy of electron-transfer reactions in polar solvents., J. Chem. Phys. 120 (2004) 7532–56.

[24] A. Chaumont, G. Wipff, Polyoxometalate Keggin Anions at Aqueous Interfaces with Organic Solvents, Ionic Liquids, and Graphite: a Molecular Dynamics Study, J. Phys. Chem. C. 113 (2009) 18233–18243.

[25] A. Chaumont, G. Wipff, Interactions between Keggin Anions in Water: The Higher Their Charge, the Higher Their Condensation? A Simulation Study, Eur. J. Inorg. Chem. 2013 (2013) 1835–1853.

[26] I.K. Song, M.S. Kaba, K. Nomiya, R.G. Finke, M. a. Barteau, Scanning tunneling microscopy (STM) and tunneling spectroscopy (TS) studies of polyoxometalates (POMs) of the Wells–Dawson structural class, J. Mol. Catal. A Chem. 262 (2007) 216–226.

[27] M.H. V Huynh, T.J. Meyer, Proton-coupled electron transfer., Chem. Rev. 107 (2007) 5004–64.